MODELING, IDENTIFICATION AND CONTROL, 2002, VOL. 23, NO. 2, 135–147
doi:10.4173/mic.2002.2.4

One-Dimensional Simulation of Clay Drying*

MARTIN SILJAN and MORTEN CHR. MELAAEN†

Keywords: *Clay, drying, simulation, LECA, LWA, porous, rotary kiln*

Drying of clay is simulated by a one-dimensional model. The background of the work is to form a better basis for investigation of the drying process in production of clay-based building materials.

A model of one-dimensional heat and mass transfer in porous material is used and modified to simulate drying of clay particles. The convective terms are discretized by first-order upwinding, and the diffusive terms are discretized by central differencing. DASSL was used to solve the set of algebraic and differential equations.

The different simulations show the effect of permeability, initial moisture content and different boundary conditions. Both drying of a flat plate and a spherical particle are modelled.

Introduction

In production of clay-based building materials, such as bricks or lightweight aggregates (LWA), the drying of the clay is an important and energy consuming part of the process. The drying is done in several different ways, e.g. in a rotary kiln, hot clay mill, tunnel kiln, or on a 'thin plate dryer'. The basis for this work is the production of LWA, with a rotary kiln drying process, Figure 1. The clay enters the

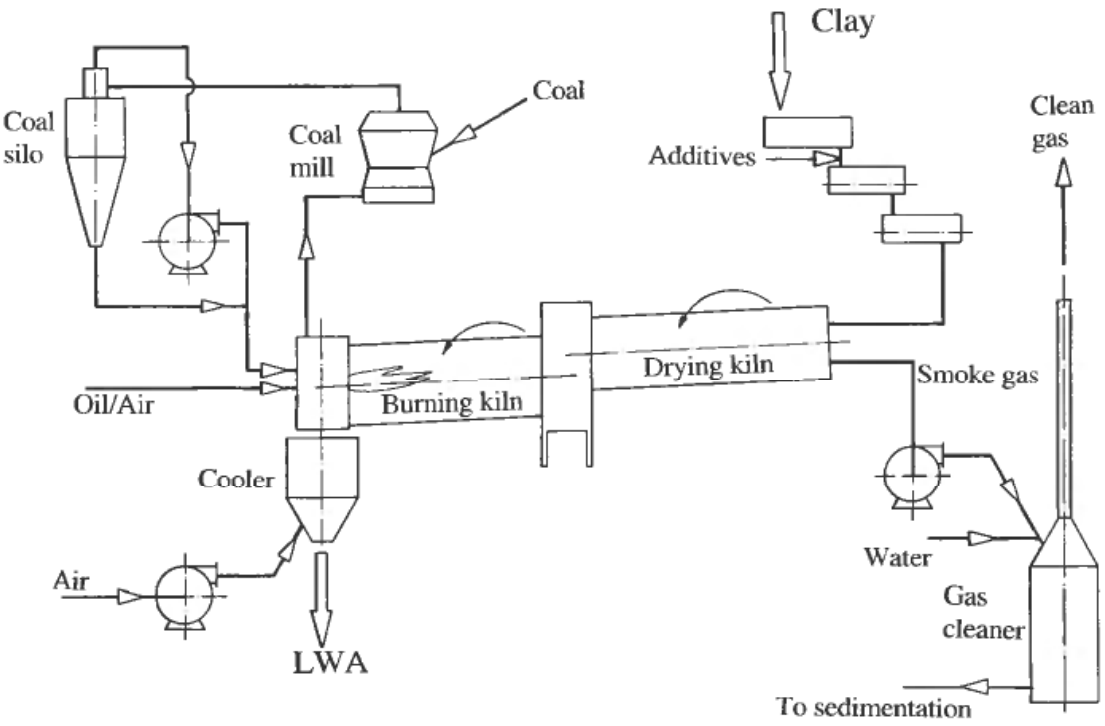

Figure 1. Simplified flow sheet for the LWA production process.

*An early version of this article was presented at the SIMS 2001 conference, October 8th–9th, Porsgrunn, Norway.

†Telemark University College (HiT-TF) and Telemark R&D Centre (Tel-Tek), Kjølnes Ring 56, 3917 Porsgrunn, Norway. Morten.C.Melaaen@hit.no

drying kiln in portions of 0–100 kg, depending on type of clay, moisture content, clay pre-treatment etc. The wet clays will stick together and form larger surfaces in the beginning of the kiln, while it towards the end of the drying will be split up into smaller pieces with diameter 0–3 cm. It is therefore interesting to investigate the drying process of both a flat clay plate and spherical clay pellet.

This investigation focuses on drying of clay used for production of *Light Weight Aggregates* (LWA). LWA is also known as *Light Expanded Clay Aggregates* (LECA).

The production process: The clay is homogenised by mixing, and eventually added some additives to improve flow- and expansion properties. It is then fed into a drying kiln, which is a slowly rotating tube (diameter: 2.5–3.4 m, length: 35–43 m, rotation speed: 1.5–3 rpm). The clay flows in counter flow with hot flue gas. Inside the tube there are various internals to control the clay flow, split up the clay into aggregates and improve heat transfer between the hot flue gas and the clay. In the drying kiln, the water is evaporated, and the clay is heated to between 250°C and 600°C.

From the drying kiln, the clay is directly transferred into the burning kiln, which is a shorter tube (diameter: 3.4–3.8 m, length: 22–28 m, rotation speed: 2–5 rpm). There are no internals in the burning kiln, except from stone lifters in the flame zone. The clay is heated to 1100–1200°C, where it expands about 300%. It is then cooled, and we have LWA.

There are basically two ways of drying out a porous media; either reduce the vapour pressure in the surroundings or transfer energy to the surface, or both. Concerning LWA-production, it is obvious that the energy transfer is the driving force of the drying process. LWA is used for several purposes, mainly LECA blocks, chimneys and as aggregates for insulation. It is also used for water filtration (Filtralite).

Simulations

The three models mostly used for simulating drying of a porous material (the rigorous model, the diffusion model and the characteristic drying curve model) were compared by Fyhr and Kemp (1998). They found that all three models gave good results for drying below the boiling point. But as the two last ones does not account for internal overpressure, only the rigorous model is suited for drying above the boiling point. It is therefore chosen here.

The model used here is one-dimensional and includes heat and mass transfer in a porous material. It is modified to simulate drying of clay. The model is based on earlier work by Whitaker (1977), Ouelhazi *et al.* (1992), Perre *et al.* (1993), Chan (1983), Chan *et al.* (1985), Glaister (1987) Krieger-Brockett and Glaister (1988), Lai (1991). A similar model has earlier been used for simulation of drying and pyrolysis of wood (Melaaen 1996) and pyrolysis of coke (Jacobsen 1997).

The model solves conservation equations for energy, liquid free water, bound water, air and vapour. The most important assumptions are 1) all phases have the same temperature, 2) the vapour pressure is equal to the equilibrium pressure, 3) transport of bound water is modeled as a diffusion process by Fick's law, 4) binary diffusion in the gas phase, 5) Darcy's law is used for the bulk flow of the gas mixture and the free liquid water and 6) shrinkage and cracking is not included in the model.

About assumption 6: Evans and Keey (1998) found the drying induced shrinkage of Hyde clay to stop at a moisture content of about 16%. Most of the simulations in this article are below this limit. Itaya *et al.* (1997) found no significant difference between the results from drying models with and without shrinkage included when

the shrinkage was of the order 0.9. Kishidaira and Watanabe (1996) found thermal expansion of clay to be negligible even at high temperatures. This means that assumption 6 is only valid for compacted clay with relatively low water content. In LWA production a broad variation of clays are used, and these conditions are only valid for some of the clays. Cracking and shrinkage may be included in the model at a later stage.

Effects of permeability, initial moisture content and different boundary conditions are simulated, both with a flat plate model and a spherical model.

Equations

The clay material can be divided into four phases; solid (s), liquid free water (l), bound water (b), and gaseous (g). The sum of the volume fractions of the four phases equals 1:

$$\varepsilon_s + \varepsilon_l + \varepsilon_b + \varepsilon_g = 1 \tag{1}$$

where the volume fraction of phase γ is given by $\varepsilon_\gamma = V_\gamma / V$. The averaging variables are given by:

$$\langle \varphi \rangle = \frac{1}{V} \int_{V_\gamma} \varphi dV, \qquad \langle \varphi \rangle^\gamma = \frac{1}{V_\gamma} \int_{V_\gamma} \varphi dV \tag{2}$$

where $\langle \varphi \rangle$ is named the phase average, and $\langle \varphi \rangle^\gamma$ is named the intrinsic phase average.

If the mass of the vapour is neglected, the total moisture content on dry basis is:

$$M = \frac{\langle \rho_b \rangle + \langle \rho_l \rangle}{\langle \rho_s \rangle} \tag{3}$$

The point where the clay contains the maximum amount of bound water, but no free water is called the moisture saturation point, M_{msp}. M_b is the amount of bound water, while M_l is the amount of free water.

Mass conservation equations

General conservation equation in the gas phase:

$$\frac{\partial}{\partial t}(\varepsilon_g \langle \rho_i \rangle^g) + \nabla \cdot \langle \rho_i \mathbf{V}_i \rangle = \langle \dot{\omega}_i \rangle \tag{4}$$

where

$$\langle \rho_i \mathbf{V}_i \rangle = \langle \rho_i \rangle^g \langle \mathbf{V}_g \rangle - \langle \rho_g \rangle^g D^i_{eff} \nabla \left[\frac{\langle \rho_i \rangle^g}{\langle \rho_g \rangle^g} \right] \tag{5}$$

For the vapour:

$$\frac{\partial}{\partial t}(\varepsilon_g \langle \rho_v \rangle^g) + \nabla \cdot \langle \rho_v \mathbf{V}_v \rangle = \langle \dot{\omega}_v \rangle \tag{6}$$

For the air:

$$\frac{\partial}{\partial t}(\varepsilon_g \langle \rho_a \rangle^g) + \nabla \cdot \langle \rho_a \mathbf{V}_a \rangle = 0 \tag{7}$$

For the liquid free water:

$$\frac{\partial \langle \rho_l \rangle}{\partial t} + \nabla \cdot \langle \rho_l \mathbf{V}_l \rangle = \langle \dot{\omega}_l \rangle, \qquad \langle \rho_l \mathbf{V}_l \rangle = \langle \rho_l \rangle^l \langle \mathbf{V}_l \rangle \tag{8}$$

For the bound water

$$\frac{\partial\langle\rho_b\rangle}{\partial t}+\nabla\cdot\langle\rho_b\mathbf{V}_b\rangle=\langle\dot{\omega}_b\rangle,\qquad\langle\rho_b\mathbf{V}_b\rangle=-\langle\rho_s\rangle D_b\nabla\left[\frac{\langle\rho_b\rangle}{\langle\rho_s\rangle}\right] \tag{9}$$

For the production terms, we have the following relation:

$$\langle\dot{\omega}_v\rangle=-(\langle\dot{\omega}_l\rangle+\langle\dot{\omega}_b\rangle) \tag{10}$$

Energy equation

All phases are assumed to have the same temperature, and thus the energy equation becomes:

$$\langle\rho C_p\rangle\frac{\partial\langle T\rangle}{\partial t}+\left(C_p(l)\langle\rho_l\mathbf{V}_l\rangle+C_p(l)\langle\rho_b\mathbf{V}_b\rangle+C_p(g)\langle\rho_g\mathbf{V}_g\rangle+\sum_{i=v,a}C_p(i)\langle\rho_i\mathbf{U}_i\rangle\right)\cdot\nabla\langle T\rangle$$

$$=\nabla\cdot(k_{eff}\nabla\langle T\rangle)-\langle\dot{\omega}_v\rangle\Delta h_v+\langle\rho_b\mathbf{V}_b\rangle\nabla(\Delta h_{sorp}) \tag{11}$$

where

$$\langle\rho C_p\rangle=C_p(s)\langle\rho_s\rangle+C_p(l)\langle\rho_l\rangle+C_p(l)\langle\rho_b\rangle+C_p(g)\langle\rho_g\rangle, \tag{12}$$

$$\Delta h_v=\Delta h_{vap}+\Delta h_{sorp} \tag{13}$$

and

$$\langle\rho_i\mathbf{U}_i\rangle=-\langle\rho_g\rangle^g D^i_{eff}\nabla\left[\frac{\langle\rho_i\rangle^g}{\langle\rho_g\rangle^g}\right] \tag{14}$$

Momentum equation

The superficial velocities for the gas phase and the liquid free water are found directly from Darcy's law, instead of solving the complete momentum equation:

$$\langle\mathbf{V}_g\rangle=-\frac{K_gK_{rg}}{\mu_g}(\nabla\langle P_g\rangle^g-\langle\rho_g\rangle^g\mathbf{g}) \tag{15}$$

$$\langle\mathbf{V}_l\rangle=-\frac{K_lK_{rl}}{\mu_l}(\nabla\langle P_l\rangle^l-\langle\rho_l\rangle^l\mathbf{g}) \tag{16}$$

$$\langle P_l\rangle^l=\langle P_g\rangle^g-P_c \tag{17}$$

Thermodynamic relations/algebraic equations

According to van der Zenden *et al.* (1996b), the equilibrium between liquid and vapour phase in a porous material is established almost instantly (10^{-4} s or less), and equilibrium is thus assumed.

$$\langle P_v\rangle^g=\langle P_v\rangle^g_{eq}(T,M)=\begin{cases}P_v^{sat}(T) & \textit{If liquid free water is present}\\ P_v^{sat}(T)h(M_b,T) & \textit{If no liquid free water is present}\end{cases} \tag{18}$$

The saturated vapour pressure and relative humidity is given by Lai (1991):

$$P_v^{sat}(T) = 101325e^{17.58-5769/T-5.686\cdot 10^{-3}T}\, N/m^2 \tag{19}$$

$$h(M_b, T) = 1 - e^{-7.05(T-273.15)^{0.4}M_b^{1.5}} \tag{20}$$

Spolek and Plumb (1981) gives the capillary pressure as

$$P_c = 1.364\cdot 10^2(128 - 0.186T)(M_l + 1.2\cdot 10^{-4})^{-0.63}\, N/m^2 \tag{21}$$

The sum of the partial densities is equal to the total density

$$\langle \rho_g \rangle^g = \sum_i \langle \rho_i \rangle^g \tag{22}$$

Further, the gaseous mixture is seen as a mixture of ideal gases:

$$\langle P_g \rangle^g = \frac{\langle \rho_g \rangle^g R_0 \langle T \rangle}{M_g} \tag{23}$$

where M_g is the average molecular weight of the gaseous mixture, defined by:

$$M_g - \left(\sum_i \frac{\langle \rho_i \rangle^g}{\langle \rho_g \rangle^g M_i} \right)^{-1} \tag{24}$$

The diffusion coefficients are given by Perre *et al.* (1993):

$$D_{eff}^i = \frac{8.803\cdot 10^{-5}\left(\dfrac{T^{1.81}}{P}\right)}{50}\, m^2/s \tag{25}$$

$$D_b = e^{-9.9+9.8M_b(4300/T)} m^2/s \tag{26}$$

Vapourization and sorption enthalpies are given by Ouelhazi *et al* (1992):

$$\Delta h_{vap} = 3174.9 - 2.46T \tag{27}$$

$$\Delta h_{sorp} = 0.4\Delta h_{vap}\left[\frac{(M_{msp} - M_b)}{M_{msp}}\right]^2 \tag{28}$$

The models for capillary pressure, sorption enthalpy and bound water diffusion are originally developed for wood, and should be investigated more with respect to the clay material.

Initial and boundary conditions

Energy transfer boundary condition:

$$\begin{aligned}&(k_{eff}\nabla\langle T\rangle + \langle \rho_l \mathbf{V}_l\rangle \Delta h_l + \langle \rho_b \mathbf{V}_b\rangle \Delta h_b)\cdot \mathbf{n}|_s \\ &= F - h_T(\langle T\rangle_s - \langle T\rangle_\infty) - \omega_s\sigma(\langle T\rangle_s^4 - \langle T\rangle_\infty^4)\end{aligned} \tag{29}$$

Table 1. Variables to be calculated

Variable	Unit	Description
$\langle T \rangle$	K	Temperature
$\langle P_g \rangle^g$	Pa	Gas phase pressure
$\langle \rho_g \rangle^g$	kg/m^3	Gas phase intrinsic density
$\langle \rho_i \rangle^g$	kg/m^3	Intrinsic density of each component in the gas phase; $i = a, v$
$\langle \rho_w \rangle$	kg/m^3	Total water density (liquid free($\langle \rho_l \rangle$) + bound($\langle \rho_b \rangle$)). Vapour ignored here.
ε_g	—	Gas phase volume fraction

Moisture transfer boundary condition:

$$(\langle \rho_l \mathbf{V}_l \rangle + \langle \rho_b \mathbf{V}_b \rangle + \langle \rho_v \mathbf{V}_v \rangle) \cdot \mathbf{n}|_s = h_m(\langle \rho_v \rangle_s^g - \langle \rho_v \rangle_\infty^g) \tag{30}$$

Pressure boundary condition:

$$\langle P_g \rangle_s^g = \langle P_g \rangle_\infty^g \tag{31}$$

Variables and equations to be solved

Variables to be calculated are given in Table 1. This means seven unknown variables.

Equations to be solved

The following equations are solved:

- Energy equation (equation 11)
- Pressure constraint based on the ideal gas equation (equation 23 together with equation 24)
- Gas intrinsic density (equation 22)
- Conservation equation for the air. (equation 7).
- Equation for the total water content by combining the equations for the vapour, bound and liquid free water

$$\frac{\partial}{\partial t}(\langle \rho_l \rangle + \langle \rho_b \rangle + \varepsilon_g \langle \rho_v \rangle^g) + \nabla \cdot (\langle \rho_l \mathbf{V}_l \rangle + \langle \rho_b \mathbf{V}_b \rangle + \langle \rho_v \mathbf{V}_v \rangle) = 0 \tag{32}$$

- Vapour density from equilibrium uses the ideal gas law together with equation 9.
- Equation for the volume fractions (equation 1) to find ε_g. Other volume fractions are given by

$$\varepsilon_s = \frac{\langle \rho_s \rangle}{\langle \rho_s \rangle^s}, \quad \varepsilon_l = \frac{\langle \rho_l \rangle}{\langle \rho_l \rangle^l}, \quad \varepsilon_b = \frac{\langle \rho_b \rangle}{\langle \rho_b \rangle^b} \tag{33}$$

This gives seven equations, and thus the number of equations corresponds to the number of unknown variables.

Numerical Solution Procedure

The grid is one-dimensional and fixed in space. The convective terms are discretized by first-order upwinding, and the diffusive terms are discretized by central differencing. DASSL was used to solve this set of algebraic and differential equations on the form

$$F\left(t, \varphi, \frac{\partial \varphi}{\partial \varphi}\right) = 0 \tag{34}$$

The initial values of φ, $\partial\varphi/\partial t$ must be given as input to DASSL, and they must be consistent. The easiest way to do this is often to do a time step with the steady-state solution, use these values as initial values, and then change the boundary conditions before the calculations proceeds.

The reason for using DASSL instead of a ready-to-use package is a wish to have full freedom with respect to the numerical solution procedure, but more important is the reason that computer programs, like CFD (Computational Fluid Dynamics) programs, do not include phase equilibrium.

Results

The permeability of air and water in different clays have been measured by Lapierre *et al.* (1990), Pusch and Schomburg (1999), Schacelford and Javed (1991), Shishido *et al.* (1992) and van der Zanden *et al.* (1996a), and have been found to be in the area 1.0e–19 to 2.9e–16 m^2.

The porosity of clays are found to be 0.25–0.4 by Silva & al. (2000), Su (1997) and van der Zanden & al. (1996a, 1996b). Tests on clay for LWA production show a porosity of 0.33 after drying. The intrinsic heat capacity is found to be 815 J/kgK and the intrinsic thermal conductivity is found to be 2.2 W/mK by Su (1997). The intrinsic density is found to be 2570–2750 kg/m^3 by Evans and Keey (1975), Silva *et al.* (2000) and Su (1997).

The bound water content and sorption enthalpy is found by Blanchart *et al.* (1995), Gong *et al.* (1998) and Khalfi and Blanchart to be strongly dependent on clay composition, both concerning minerals, impurities and particle size distribution. In Table 2 the selected physical parameters and initial values are shown.

The different parameters and initial values are varied individually as deviations from the standard case, and thus co-variations are not simulated. The spherical model is used as standard case when nothing else is specified. Results from the simulations are given in Figures 2–8.

Table 2. Physical parameters and initial values in the model. Highlighted figures indicate standard case

Physical parameter/initial value	Values used	Unit
Permeability of air and water	1, 5, 10, **50**, 100, 500, 1000	10^{-19} m^2
Porosity	**0.33**	—
Intrinsic heat capacity	**815**	J/kgK
Intrinsic density	**2650**	kg/m^3
Intrinsic thermal conductivity	**2.2**	W/mK
Bound water content	**130**	kg/dm^3
Total water content	50, **100**, 150, 200, 250	kg/dm^3
Radius (spherical model)	0.002, 0.005, **0.01**, 0.02, 0.05	m
Plate thickness (flat plate model)	0.002, 0.005, **0.01**, 0.02, 0.05	m
Initial temperature	**300**	K
Surroundings temperature	350, 400, 450, **500**, 550, 600	K
Heat transfer number	**5**	W/m^2K
Mass transfer number	**1**	m/s
Incident heat flux	**0**	W/m^2

Figure 2 shows the temperature distribution in a clay pellet during drying. Figure 3 and 4 shows the water content in both a clay pellet (a) and a flat clay plate (b) during drying. Figure 5 shows the effect of sample size, both for a pellet (a), and for a flat plate (b). Figure 6 shows the effect of permeability in the clay (a) and the surroundings temperature (b). Figure 7 shows the water content in a pellet during drying, with both free and bound water present. Figure 8 sums up Figure 5–7.

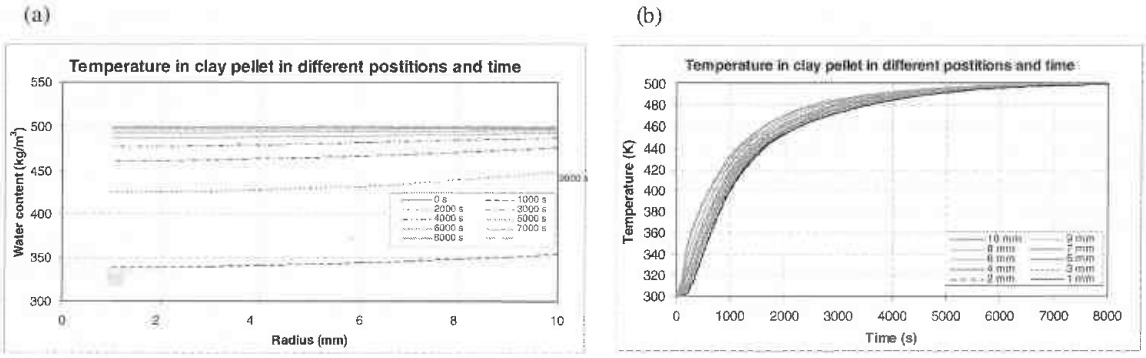

Figure 2. Results from simulation of drying of a spherical clay pellet with radius 1 cm at standard conditions/parameters (see Table 2). The figures show temperature variations in different positions and time. The label in Figure (a) indicates time, and (b) radius position.

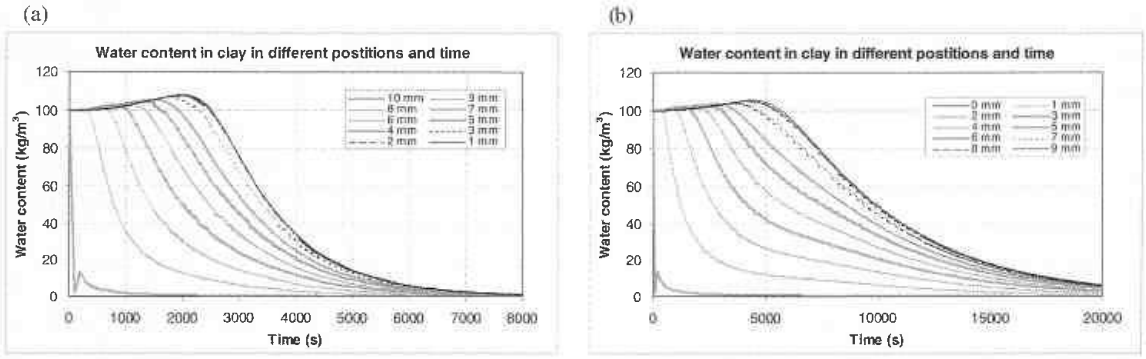

Figure 3. Results from simulation of drying of (a) a spherical clay pellet with radius 1 cm and (b) a clay plate with thickness 1 cm, at standard conditions/parameters (see Table 2). The figures show the water content in different positions and time. The label in Figure (a) indicates radius position, and (b) the distance from surface.

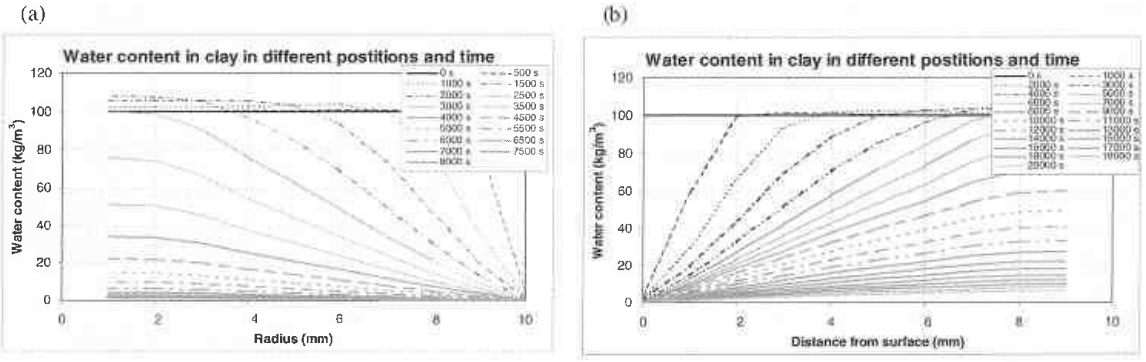

Figure 4. Results from simulation of drying of (a) a spherical clay pellet with radius 1 cm and (b) a clay plate with thickness 1 cm, at standard conditions/parameters (see Table 2). This figure is based on the same data as Figure 3, but here each line represents a moment in time instead of a position in the material.

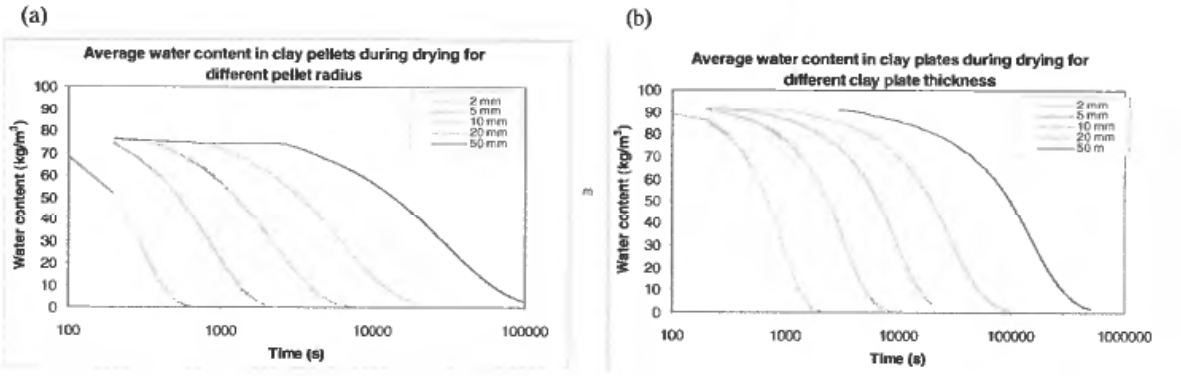

Figure 5. Results from simulation of drying of (a) spherical clay pellets with different radius and (b) clay plates with different thickness, at standard conditions/parameters (see Table 2). Each line represents a different pellet or plate.

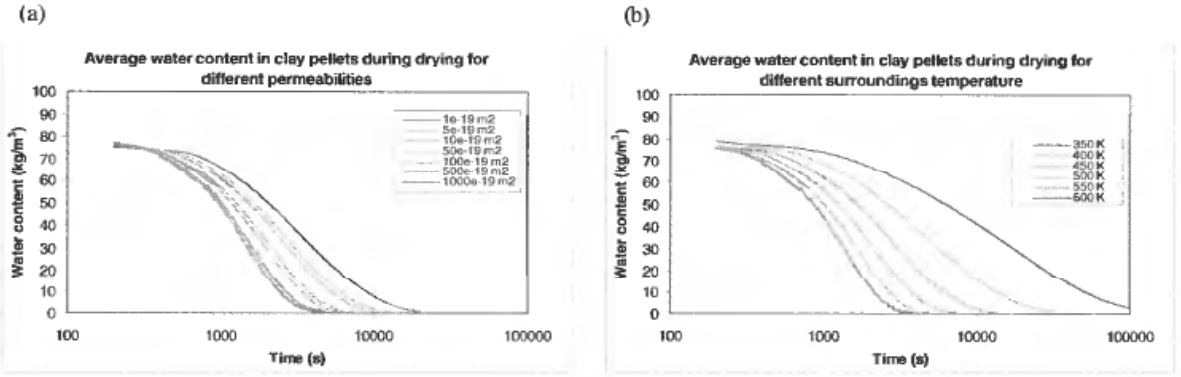

Figure 6. Results from simulation of drying of a spherical clay pellet with (a) different permeability and (b) different surroundings temperature, at standard conditions/parameters (see Table 2). Each line represents different conditions.

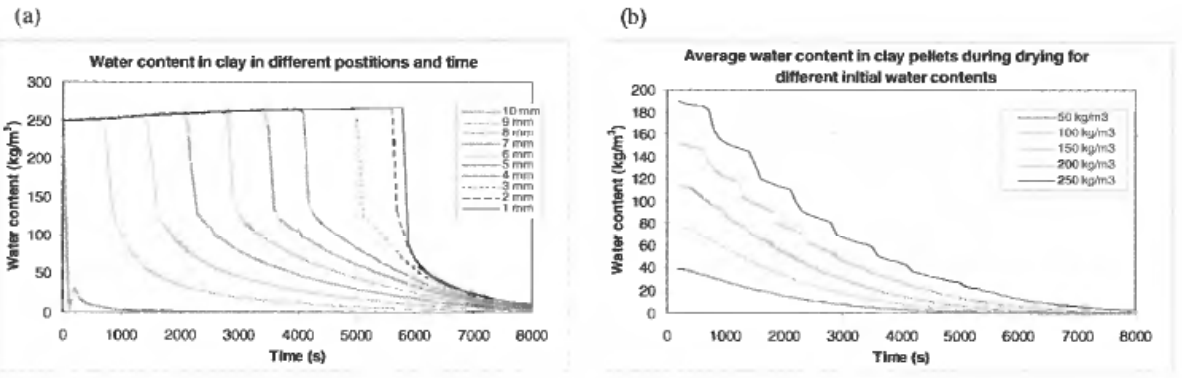

Figure 7. Results from simulation of drying of a spherical clay pellet with radius 1 cm with bound and free water. The figures show drying of a pellet with (a) initial water content at 250 kg/m^3, (b) different initial water contents at standard conditions/parameters (see Table 2). The figures show the water content in different position and time. The label in figure (a) indicates radius position, and in figure (b) initial water content.

As we can see from Figure 2, the temperature gradients in the pellet are not very large. Especially Figure 2(a) shows a relatively flat temperature profile. From Figure 3 and 4 we can see that the gradients regarding water content are much larger than for temperature. In both these cases, the initial water content is 100 kg/m^3. As a

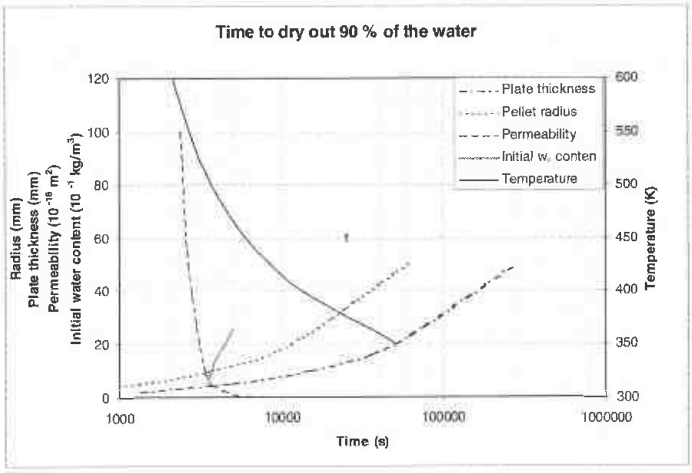

Figure 8. The figure shows time to dry out 90% of the water in the clay, with variations of plate thickness (cartesian model), radius (spherical model), permeability (spherical model), initial water content (spherical model) and surroundings temperature (spherical model). The variations are done as deviations from the standard case (see Table 2), and sums up Figures 5–7.

result of water diffusing inward into the sample and condensing, the local water content exceeds this value. As expected, the pellet is dried out faster than the plate.

Figure 5 shows how the drying time increases with sample size. As expected, increased dimensions of the object prolong the drying time. Figure 6 (a) shows that lower permeability and lower surroundings temperature increases the drying time, as expected.

Figure 7 shows the drying process when both free and liquid water is present. Figure (a) shows a steep drying front when going from liquid free water to bound water. As expected, higher initial water content means longer drying time as seen in Figure (b). The oscillations in Figure (b) may be caused by too coarse grid.

From Figure 8 we can see that the sample size and surroundings temperature is very important for the drying time, as expected. The dependence upon permeability is also as expected. When the permeability is high, the drying process will be more controlled by energy transfer. The dependence upon initial moisture content is maybe a little less than expected.

Conclusions

The necessary equations and sub models describing drying of clay both with bound and liquid free water are given. The equation system with differential and algebraic equations is solved for one-dimensional transient problems of spherical and plate shape. The convective terms are discretised by first-order upwinding, while central differencing is used for the diffusive terms. The program code DASSL is used for integrating the equation system in time.

The results are mostly as expected. The drying time is rather high, about two hours for a spherical clay pellet with diameter 2 cm (see Figure 2(a)), but it must be remember that this is compact clay with no cracks. The drying time is also very dependent upon surroundings temperature and sample size (see Figures 5–6), as expected. The dependence upon initial moisture content is maybe a little less than expected.

Further Work

The most important improvements to the model would be to include cracking and shrinkage. Some of the clays used for LWA production have initial water content as high as 500 kg/m^3, and thus shrinkage and cracking obviously occurs. To develop good models will require more knowledge about clay behaviour during drying.

Further, the model experiences some difficulties when the porous material is close to completely saturated with liquid. This is caused by the numerical solution procedure, when the material gets 'over-saturated' as a result of temporarily inaccuracies.

The models for capillary pressure, sorption enthalpy and bound water diffusion are originally developed for wood, and should be investigated more with respect to the clay material.

Nomenclature

Symbol	Unit	Description
ε	—	Volume fraction
$\mathbf{V}$	m/s	Superficial velocity
V	m^3	Volume
φ	—	General variable
$\langle\varphi\rangle$	—	Average value of φ
$\langle\varphi\rangle^{\gamma}$		Average value of φ in phase γ
M	—	Moisture content
M_{msp}	—	Moisture saturation point
t	s	Time
ρ	kg/m^3	Density
$\langle\dot{\omega}_i\rangle$	kg/m^{3}s	Production rate of component or phase i
D^i_{eff}	m^2/s	Effective diffusivity of component I in gas mixture
T	K	Temperature
C_p	J/kgK	Specific heat capacity at constant pressure
$\mathbf{U}$	m/s	Diffusion velocity
k_{eff}	W/mK	Effective thermal conductivity
Δh_v	J/kg	Vapourization enthalpy + sorption enthalpy
Δh_{vap}	J/kg	Vapourization enthalpy
Δh_{sorp}	J/kg	Sorption enthalpy
K	m^2	Intrinsic permeability
K_r	—	Relative permeability
$\mathbf{g}$	m/s^2	Gravity
P	N/m^2	Pressure
D_b	m^2/s	Diffusivity of bound water
X_b	—	Mass fraction of bound water
$h(M_b,T)$	—	Relative humidity
R_0	J/molK	Universal gas constant
F	W/m^2	Incident heat flux to surface
$\mathbf{n}\|_s$	—	Unit normal vector with direction out of surface
ω_s	—	Emissivity
σ	W/m^{2}K^4	Stefan-Bolzman constant
h_m	m/s	Mass transfer number
l	—	Liquid water phase
b	—	Bound water phase
g	—	Gas phase
s	—	Solid phase
μ	kg/ms	Dynamic viscosity

Superscript or subscript	Description
l	Liquid water (phase)
b	Bound water (phase)
g	Gas (phase)
s	Solid (phase)
v	Vapour
a	Air
γ	Random phase
I	Random component
sat	Saturated
∞	Ambient

References

Ben Nasrallah, S. and Perre, P. (1988). Detailed study of a model of heat and mass transfer during convective drying of porous media, *Int. J. Heat Mass Transfer*, 31(5), pp. 957–967.

Blanchart, P., Gaillard, J. M. and Weber, F. (1995). The drying of clay-minerals and mixed clay-minerals, *Journal of Material Science*, 30, pp. 2319–2324.

Chan, W. C. R. (1983). *Analysis of chemical and physical process during the pyrolysis of large biomass pellets*, Ph.D. Thesis, University of Washington, Seattle, WA.

Chan, W. C. R., Kelbon, M. and Krieger-Brockett, B. (1985). Modeling and experimental verification of physical and chemical process during pyrolysis of large biomass particle, *Fuel*, 64, pp. 1505–1513.

Evans, A. A and Keey, R. B. (1975). The moisture diffusion coefficient of a shrinking clay on drying, *The Chemical Engineering Journal*, 10, pp. 127–134.

Fyhr, C. and Kemp, I. C. (1998). Comparison of different drying kinetics models for single particles, *Drying Technology*, 16, pp. 1339–1369.

Glaister, D. S. (1987). *The prediction of chemical kinetic, heat and mass transfer process during the one- and two-dimensional pyrolysis of a large wood pellet*, M.Sc. Thesis, University of Washington, Seattle, WA.

Gong, Z. X., Mujumdar, A. S., Itaya, Y., Mori, S. and Hasatani, M. (1998). Drying of clay and nonclay media: Heat and mass transfer and quality aspects, *Drying Technology*, 16, pp. 1119–1152.

Itaya, Y., Taniguchi, S. and Masanobu, H. (1997). A numerical study of transient deformation and stress behavior of a clay slab during drying, *Drying Technology*, 15, pp. 1–21.

Jacobsen, M. (1997). *Heat and mass transfer in a vertical flue ring furnace*, Doktor ingeniøravhandling, NTNU.

Khalfi, A. and Blanchart, P. (1996). Desorption of water during the drying of clay minerals. Enthalpy and entropy variation., *Ceramics International*, 25, pp. 409–414.

Kishidaira, K. and Watanabe, K. (1996). Hygrothermal stress of clay in a high-speed drying furnace, *Journal of Thermal Stresses*, 19, pp. 599–612.

Krieger-Brockett, B. and Glaister, D. S. (1988). Wood devolatilisation—Sensitivity to feed properties and process variables. In: *Research in Thermochemical Biomass Conversion*, Bridgewater, A. V., Ed., pp. 127–142.

Lai, W.-C. (1991). *Reaction engineering of heterogeneous feeds: Municipal solid waste as a model*, Ph.D. Thesis, University of Washington, Seattle, WA.

Lapierre, C., Lerouel, S. and Locat, J. (1990). Mercury intrusion and permeability of Louisville clay, *Can. Geotech. J.*, 27, pp. 761–773.

Melaaen, M. C. (1996). Numerical analysis of heat and mass transfer in drying and pyrolysis of porous media, *Numerical Heat Transfer*, 29, pp. 331–335.

Ouelhazi, N., Arnaud, G. and Fohr, J. P. (1992). A two dimensional study of wood plank drying. The effect of gaseous pressure below boiling point, *Transp. Porous Media*, 7, pp. 39–61.

PERRE, P., MOSER, M. and MARTIN, M. (1993). Advances in transport phenomena during convective drying with superheated steam and moist air, *Int. J. Heat Mass Transfer*, 36, pp. 2725–2746.

PUSCH, R., SCHOMBURG, J. (1999). Impact of microstructure on the hydraulic conductivity of undisturbed and artificially prepared smectitic clay, *Engineering Geology*, 54, pp. 167–172.

SCHACELFORD, C. D. and JAVED, F. (1991). Large-scale laboratory permeability testing of a compacted clay soil, *Geotechnical Testing Journal*, 14(2), pp. 171–179.

SHISHIDO, I., SUZUKI, M. and OHTANI, S. (1992). On the drying mecanism of shrinkage materials, *Drying Technology*, 10, pp. 563–589.

SILVA, M. A., KERKHOF, P. J. A. M. and COUMANS, W. J. (2000). Estimation of effective diffusivity in drying of heterogeneous porous media, *Ind. Eng. Chem. Res.*, 30, pp. 1443–1452.

SPOLEK, G. A., PLUMB, O. A. (1981). Capillary pressure in softwoods, *Woods Sci. Technol.*, 15, pp. 189–199.

SU, S.-L. (1997). Modeling of multi-phase moisture transfer and induced stress in drying clay bricks, *Applied Clay Science*, 12, pp. 189–207.

VAN DER ZANDEN, A. J. J., COUMANS, W. J., KERKHOF, P. J. A. M and SCHOENMAKERS, A. M. E (1996). Isotermal moisture transport in partially saturated porous media, *Drying Technology*, 14, pp. 1525–1542.

VAN DER ZANDEN, A. J. J., SCHOENMAKERS, A. M. E., KERKHOF, P. J. A. M. (1996). Isotermal vapour and liquid transport inside clay during drying, *Drying Technology*, 14, pp. 647–676.

WITHAKER, S. (1977). Simultaneous heat , mass and momentum transfer in porous media: A theory on drying. *Adv. Heat Transfer*, 13, pp. 119–203.